

Supernovae Simulations and Strategies: Application to the Dark Energy Survey (Draft: October 26, 2010)

J. P. Bernstein¹, R. Kessler^{2,3}, S. Kuhlmann¹, R. Reis⁴,
I. Crane^{1,5}, D. A. Finley⁴, J. A. Frieman^{2,3,4}, T. Hufford¹, A. G. Kim⁶, J. Marriner⁴,
P. Mukherjee⁷, R. C. Nichol⁸, P. Nugent⁶, D. R. Parkinson⁷, M. Sako⁹, H. Spinka¹. . .

ABSTRACT

We present an analysis of Type Ia supernova light curves simulated for the upcoming Dark Energy Survey (DES) supernova search. Employed is a code suite that generates and fits realistic supernova light curves in order to obtain distance modulus/redshift pairs which are passed to a cosmology fitter. We harnessed the fit results to investigate several different survey strategies including field selection, supernovae selection biases, and photometric redshift measurements. We forecast that the DES supernova search will discover on the order of 6000 Type Ia supernovae, with ~ 3000 passing selection cuts, with planned full spectroscopic host galaxy follow-up out to a redshift of 1. Thus, the DES will provide by far the largest self-contained, high-redshift Type Ia sample to date, and will significantly improve z -band coverage relative to SNLS due to the heightened red sensitivity of the DES camera. Prior to obtaining host spectra, our analysis during survey operations will rely on photometric redshifts. Our simulations predict that for the DES, the distribution of photometric minus true supernova redshift will have a width of less than 3 percent and minimal non-Gaussian tails when the host galaxy photometric redshift is used as a prior. We further present estimates of 1) systematic effects on DES supernova observations and 2) the Dark Energy Task Force figure of merit.

Subject headings: supernovae – cosmology: simulations

¹Argonne National Laboratory, 9700 South Cass Avenue, Lemont, IL 60439, USA

²Kavli Institute for Cosmological Physics, The University of Chicago, 5640 South Ellis Avenue Chicago, IL 60637, USA

³Department of Astronomy and Astrophysics, The University of Chicago, 5640 South Ellis Avenue Chicago, IL 60637, USA

⁴Center for Particle Astrophysics, Fermi National Accelerator Laboratory, P.O. Box 500, Batavia, IL 60510, USA

⁵Department of Physics, University of Illinois at Urbana-Champaign, 1110 West Green Street, Urbana, IL 61801-3080 USA

⁶E. O. Lawrence Berkeley National Laboratory, 1 Cyclotron Rd., Berkeley, CA 94720, USA

⁷Department of Physics and Astronomy, Pevensey 2 Building University of Sussex, Falmer Brighton BN1 9QH, UK

⁸Institute of Cosmology and Gravitation, Mercantile

1. Introduction

Observations of distant Type Ia supernovae (SNe) provided the first evidence for the acceleration of cosmic expansion in the late 1990's (Riess et al. 1998; Perlmutter et al. 1999). Dedicated SN surveys such as the ESSENCE Supernova Survey (Miknaitis et al. 2007; Wood-Vasey et al. 2007), Supernovae Legacy Survey (SNLS, Astier et al. 2006), Sloan Digital Sky Survey-II Supernova Survey (SDSS-IISS, Frieman et al. 2008b), Supernova Cosmology Project (SCP, Perlmutter et al. 1999), Carnegie Supernova Project (CSP,

House, Hampshire Terrace, University of Portsmouth PO1 2EG, UK

⁹Department of Physics and Astronomy, University of Pennsylvania, 203 South 33rd Street, Philadelphia, PA 19104, USA

Hamuy et al. 2006), and Hubble Higher-z Supernova Search (HHZSS, Strolger et al. 2004) have substantially improved the quantity and quality of SNIa data in the last decade. A new energy-density component known as dark energy is the most common explanation for cosmic acceleration (for a review, see Frieman et al. 2008a). The recent SN data, in combination with measurements of the cosmic microwave background (CMB) anisotropy and baryon acoustic oscillations (BAO), have confirmed and constrained accelerated expansion in terms of the dark energy density Ω_{DE} , and the equation of state parameter, $w \equiv p_{DE}/\rho_{DE}$, where p_{DE} & ρ_{DE} are the pressure and density of dark energy, respectively. New surveys of supernovae, BAO, weak lensing, and galaxy clusters are being planned and implemented in order to improve the constraints on w .

Future supernova measurements face similar issues, such as number and position of fields, filters, exposure times, cadence, spectroscopic and photometric redshifts, etc. Each study must optimize telescope allocations to return the best cosmological constraints. The simulation analysis presented in the paper is for the Dark Energy Survey (DES¹⁰) which is on track for first light in 2011. The DES will carry out a deep optical and near-infrared survey of 5000 square degrees of the South Galactic Cap (see Fig. 1), using a new 3 deg² Charge Coupled Device (CCD) camera (“DECAM”) to be mounted on the Blanco 4-meter telescope at the Cerro Tololo Inter-American Observatory (CTIO). The supernova component of the survey will use approximately 10% of the total survey time during photometric conditions and make maximal use of the non-photometric time, for a total supernova survey of >1000 hours. The much-improved red sensitivity of the thicker CCDs (Holland 2002; Groom et al. 2006) from Lawrence Berkeley National Laboratory (LBNL) will increase the signal-to-noise ratio for the redder bands in general and for high redshift supernovae in particular.

Current SNIa data sets that include supernova spectra consist of ~ 1000 SNIa spread out over 5 surveys, approximately 300 of which have been published, with potentially three times more with photometric host redshifts but no spectroscopic

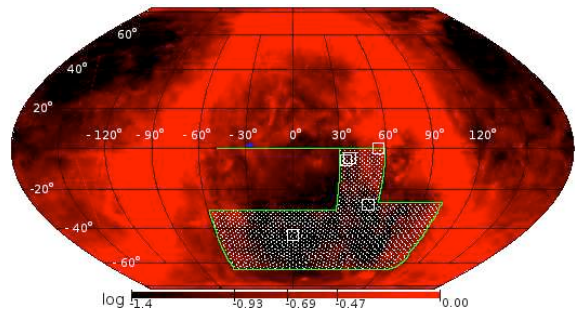


Fig. 1.—: DES survey footprint. The white squares indicate the locations of the five SN fields that are currently favored (see Tab. 3.) The size of the squares as shown is much larger than the deg² field of view of the camera in order to make them easier to see in the Figure. The scale shows the log of r -band (as defined in Tab. 2) extinction in magnitudes.

SNe confirmation. The usefulness of the current photometric samples depends on the fraction of host galaxies for which spectra are obtained (i.e., hosts “followed-up”), a number which is uncertain, and the precision of inter-survey calibrations. DES alone will identify ~ 3000 high-quality SNe that pass strong selection cuts (§3.1). The DES collaboration plans to acquire a SN spectrum near peak for $\sim 20\%$ of this sample. For the remaining $\sim 80\%$, there are two bounding redshift scenarios 1) photometric SN/host redshift determination, and 2) spectroscopic host-galaxy follow-up. In reality, the scenario will fall somewhere between these extremes. The goal of the DES is to land as close to the second scenario as possible, and the balance will be quantitatively addressed via the Dark Energy Task Force figure of merit (see §??). We recognize and are addressing the necessity for realistic simulations of host photometric redshifts as they will be needed to aid in SNIa typing, and may be required for SNe with faint hosts and hosts for which a spectrum is unobtainable. In the final analysis, DES is projected to amass by far the largest high-quality, cohesive SNIa data set to date out to a redshift of at least 1.0. This will advance the state of the art in that the single large data set will eliminate the issue of inter-calibration currently facing the multi-survey data and z -band coverage as compared to SNLS will be significantly improved due to the height-

¹⁰<http://www.darkenergysurvey.org>

ened red sensitivity of the DES CCDs (see Fig. 2).

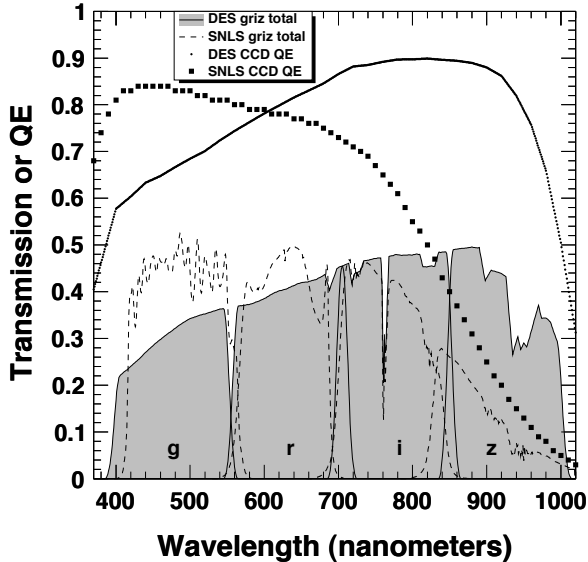


Fig. 2.—: Estimate of the comparison of the DES and SNLS filter transmission, CCD quantum efficiency (QE), and total transmission (including the effects of QE, the atmosphere, and the optical systems of the relevant cameras). The SNLS data are from Regnault et al. (2009). Highlighted are the advantage of the DES CCDs at redder wavelengths and the projected uniformity of the DES filters. Note that the SNLS curves are from actual measurements whilst the DES counterparts are generated from detailed simulations as the DES camera and filters are under construction.

In order to aid in the design of the optimal DES SN survey, we simulate DES SN observations. A pixel-level simulation would be ideal, but is prohibitively expensive in terms of computational resources due to the many iterations needed to optimize the DES SN search. We therefore use a parametric code suite called “SNANA” (Kessler et al. 2009a) that generates realistic SN light curves taking into account seeing conditions, dust extinction (Cardelli et al. 1989), detector noise, and intrinsic SN luminosity variations using MLCS2k2 (Jha et al. 2007) or SALT2 (Guy et al. 2007) models. While SNANA does not address potential artifacts in host-galaxy and sky subtraction, we note that this has been studied by the SDSS collaboration (Holtz-

man et al. 2008), and that the parametrization of the photometric errors has been shown to be reliable over a broad range of sky noise and signal-to-noise. We further employ an MLCS-based fitter to obtain the distance modulus, μ , for each SN. Sample redshifts are expected to come from a combination of SN spectra and photometric redshifts from the host galaxy and supernova, and results are compared for these different scenarios. Variations of the input parameters to the simulation are used to estimate systematic uncertainties.

The outline of the paper is as follows. We present our method of supernova light curve simulation in §2. We discuss DES survey options and present example simulations in §3, and discuss photometric redshifts and Type Ia sample contamination from core collapse SNe in §5. We present and discuss our results in §§? and §§?, respectively.

2. Supernova light curve simulation

In this section, we present our supernova light curve simulations in greater technical detail. We discuss general properties of SNANA in §2.1 and introduce our application to the DES in §2.2.

2.1. SNANA

DES is using the publicly available¹¹ SNANA (Kessler et al. 2009a) package to simulate and fit Type Ia and Type Ibc/II supernova light curves. We emphasize that while we are using SNANA to investigate the capabilities of DES, it was originally developed for the analysis of observational SDSS supernova data, is currently being used by the Large Synoptic Survey Telescope (LSST) collaboration to forecast SN observations, and can be applied to any survey in general. SNANA employs a mixture of C and FORTRAN routines to simulate and fit SN light curves for a range of redshifts (z). Using the simulation requires a survey-specific library that includes the survey characteristics, e.g., observing cadence, seeing conditions, zeropoints, CCD characteristics, etc. Survey filter properties must also be defined. Constructing this library is straight forward post-survey; predicting it before the survey is crucial to making realistic predictions of light-curve quality.

¹¹<http://www.sdss.org/supernova/SNANA.html>

SNANA can generate light curves using various models, e.g. MLCS2k2 (Jha et al. 2007) or SALT2 (Guy et al. 2007). The simulation is designed to be fast, generating a few dozen light curves per second, while still providing accurate and realistic SN light curves. The light curve fitter is more time intensive and takes up to ~ 1 minute per SN to run. We make use of two light-curve models to fit the simulated light curves: the MLCS2k2 model integrated into SNANA and the publicly available SALT2 model. The MLCS2k2 fitter is improved relative to the Jha et al. (2007) code (see §5.1 and Appendix B of Kessler et al. 2009b), and it fits in flux instead of magnitudes. For additional details of SNANA, see Kessler et al. (2009a), as well as §5 & §6 of Kessler et al. (2009b).

For a rest-frame supernova light curve model, such as MLCS2k2, the basic simulation steps are as follows:

1. pick a sky position, redshift, and sequence of observer and rest frame dates,
2. pick a random luminosity parameter and random extinction (Δ & A_V , respectively; see Jha et al. 2007; Cardelli et al. 1989) according to measured distributions,
3. generate a rest-frame light curve: magnitudes in the U , B , V , R , & I filters (Bessell 1990) vs. time,
4. add host-galaxy extinction to the $UBVRI$ magnitudes,
5. add K-corrections (Nugent et al. 2002, see below) to transform $UBVRI$ to observer-frame filters,
6. add Galactic (Milky Way) extinction using the Schlegel maps (Schlegel et al. 1998),
7. apply survey zeropoints to convert from magnitudes to flux and account for atmospheric transmission,
8. apply CCD gain and noise and use the point spread function (PSF) to compute sky noise (see the SNANA manual referenced in Kessler et al. 2009a)).

For an observer-frame mode such as SALT2, steps 3-6 are combined. For the MLCS2k2 model, K-corrections are needed in both the simulator and

fitter, and are applied using a technique very similar to that in Jha et al. (2007).

2.2. Simulation inputs

As noted in the previous section, construction of a survey-specific library as input to the supernovae simulation is crucial to obtaining realistic simulated light curves. This library includes information about the survey cadence, field RA & DEC (for implementation of Milky-Way extinction), filters, CCD gain and noise, point-spread-function (PSF), sky background level, and zeropoints and their fluctuations. The zeropoint encodes exposure time, atmospheric transmission, and telescope efficiency and aperture. These vary with each exposure and so, for the Dark Energy Survey study, we created a program which uses the CTIO weather histories, ESSENCE zeropoint and PSF data, interruptions due to Blanco community use, moon brightness, etc., to estimate the parameters for the DES simulation library. Tab. 1 shows example entries in this library, and we now discuss the details of their creation.

MJD/Filter	PSF (pixels)	Sky (e^-)	Zpt (mag)
55881.191/g	2.26	80	33.0
55881.199/r	2.16	151	34.5
55881.215/i	2.05	257	34.7
55881.238/z	1.79	651	35.6
55884.312/g	2.58	143	32.7
55884.328/r	2.62	220	34.3
55884.344/i	2.35	390	34.4
55885.188/z	2.83	764	35.7

Table 1:: Example simulation inputs for the Dark Energy Survey where “Sky” is the sky noise in photoelectrons and “Zpt” is the zeropoint in magnitudes. Additional inputs that are needed, but not shown in this table, are the RA & DEC of the field, CCD gain and noise, pixel size, and the sub-contribution to the zeropoint due to fluctuation.

The Dark Energy Survey will observe from September to February, with half-nights in January and February. DES will not observe for 9-10 days each month that are reserved for community time. We have assumed that community time will be broken into three 3-4 day periods each month, which will have the minimal impact on supernova cadence. We have integrated these community pe-

riods into our simulated cadence. The supernova component of the DES is limited to at most 10% of the total survey photometric time. An 8-day trigger, representing the optimal balance between the 10% photometric time limit and avoidance of large temporal gaps, is imposed: if a supernova field has not been observed in a given filter for 8 days, then it becomes the top observational priority of the survey. In addition, supernova fields make maximal use of non-photometric time. The separation of non-photometric and photometric time in the generation of the simulation library is accomplished by cloud camera data maintained at CTIO for more than twenty years. This supernova survey strategy leads to a two-component cadence: a peak at very short cadence due to several-day periods of non-photometric time when the supernova fields dominate the observing time, and a second peak around 8 days when photometric time is used (see Fig. 3). Our supernova observing also requires an airmass less than 2.0. This, combined with DES half-nights in January and February and long periods of photometric conditions, can lead to longer cadences.

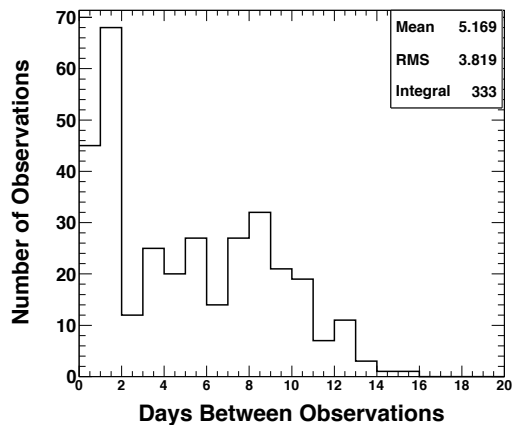


Fig. 3.—: The DES forecast for the distribution of the temporal gaps between observations during a typical DES SN season. The histogram entries are for each of the *griz* filters, e.g., a gap of 6 days in observations in any one of filters increments the count of 6-day gaps in the figure.

The other critical components of the simulation input library are the PSF, the sky background,

and the zeropoints. Usually, in this type of study, one takes averages of these quantities. In our case, we have used ESSENCE data to provide variations of PSF and zeropoints at CTIO for each observation, as well as SDSS data for the dependence of sky background on relative moon position. The measured PSF variation of ESSENCE is input directly into the simulation library after correcting for different pixel sizes, wavelength of the filter centroids, and airmasses for the mock DES observation. The resulting PSF distribution is shown in Fig. 4. Zeropoints are handled in a similar fashion. The “excess” zeropoint in the ESSENCE measurement not accounted for by airmass or exposure time is added to the nominal DES zeropoint for each filter. Tab. 1 shows example simulation inputs for two days of the DES supernova survey. The numbers correspond to the default exposure times discussed in the next section.

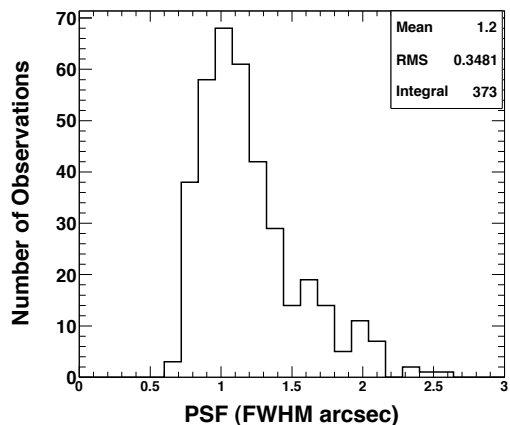


Fig. 4.—: The DES forecast for the number of observations versus the input PSF for a typical DES SN season. The histogram entries are for each of the *griz* filters, e.g., an observation with a PSF value of 1.0 in any one of filters increments the count of 1.0 PSF observations in the figure.

Another key input to the simulation is the rate of SNIa explosions in the Universe as a function of redshift. The total number of SNe DES will observe is clearly directly sensitive to that rate. The default SNIa rate we employ in SNANA is the power law from Dilday et al. (2008):

$$R_{\text{SNIa}} \equiv \text{SNIa rate} = \alpha_{\text{Ia}} \times (1+z)^{\beta_{\text{Ia}}} \quad (1)$$

Filter	Range (nm)	Exposure time (s)
<i>g</i>	400–550	300
<i>r</i>	560–710	1200
<i>i</i>	700–850	1800
<i>z</i>	850–1000	4000
<i>Z</i> ₁	850–970	<i>n/a</i>
<i>Z</i> ₂	850–920	<i>n/a</i>
<i>Y</i>	970–1020	<i>n/a</i>

Table 2:: Characteristics of the filters considered for the Dark Energy Survey. Also shown are the exposure times for a deep *griz* survey.

where $\alpha_{Ia} = (2.6+0.6-0.5) \times 10^{-5} \text{ SNe } h_{70}^3 \text{ Mpc}^{-3} \text{ yr}^{-1}$, $h_{70} = H_0 / (70 \text{ km s}^{-1} \text{ Mpc}^{-1})$, H_0 is the present value of the Hubble parameter, and $\beta_{Ia} = 1.5 \pm 0.6$. Dilday et al. (2008) further found the correlation coefficient between α_{Ia} and β_{Ia} to be -0.80 .

3. Survey options and example simulations

The current DES SN survey constraint is for 1318 hrs of total exposure time, 962 ($\sim 73\%$) of which occurs during non-photometric conditions, and there is an automatic 8-day trigger if no photometric observation has been performed for a given filter. Here we attempt to optimize the DES SN survey strategy within these constraints. For the simulations presented here, we employed the MLCS2k2 model (Jha et al. 2007) as the basis for generating and fitting SNe light curves. The free parameters are the epoch of maximum light in the *B*-band (t_o), the distance modulus (μ), the luminosity/light curve shape parameter (Δ), and the extinction in magnitudes by dust in the host galaxy (parametrized by A_V and R_V from Cardelli et al. 1989). For this study, A_V and Δ were constrained to a range of 0.0 to 2.0 and -0.4 to 1.80, respectively, and R_V was fixed to 3.1 (the average for the Milky Way). However, Kessler et al. (2009b) found the mean host galaxy reddening parameter for their 103 SNIa sample to be $R_V = 2.23 \pm 0.14(\text{stat}) \pm 0.44(\text{syst})$, and so smaller values of R_V and R_V variations are under exploration.

3.1. Filters, fields, and selection cuts

We have used SNANA to optimize the DES SN survey strategy by exploring, e.g., 1) survey depth, the 2) choice of *z* filter, 3) possible use of *Y*-band, 4) cadence, etc. We considered supernova surveys of 3 deg², 9 deg², and 27 deg² that correspond to “ultra-deep” (1 DES field), “deep” (3 DES fields), and “shallow” (9 DES fields) surveys, respectively, as the total exposure time is fixed. We also considered a hybrid survey of 15 deg² (5 DES fields) characterized by a mixture of the deep and shallow strategies. We further evaluated the *griz*, *grizY*, *grizZ*₁*Y*, and *grizZ*₂*Y* filter sets (see Tab. 2). The *griz* filters are SDSS-like and the gap between *g* and *r* is deliberate. It can be traced back to the *UVGR* system of Thuan & Gunn (1976), and was positioned to avoid the [OI] line at 5577 Å. The *Y* filter occupies the clean wavelength range between the atmospheric absorption bands at 0.95 μm and 1.14 μm, the *Z*₁ filter avoids the overlap with *Y*, and *Z*₂ avoids the *Y* overlap and the lower atmospheric absorption feature.

Our investigations showed that the choice of *z*-like filter has little effect so we selected the *z*-filter for SN observations matching the DES selection in general. Therefore, we henceforth pursued simulations using the *z* filter. In addition, our simulations show that inclusion of the *Y* filter significantly reduces the exposure time in *z* without significant benefit and, as described below, the signal-to-noise of *Y*-band measurements is limited. Therefore, the current default survey does not use the *Y* filter for supernova observations. Fig. 2 shows the chosen DES SN filters along with the DES quantum efficiency highlighting the red sensitivity (Holland 2002; Groom et al. 2006) of the relatively thicker CCDs from LBNL. Tab. 2 shows the filter exposure times for a deep *griz* survey. For the studies presented here, shallow fields have one third the exposure time for the hybrid strategy.

The choice of DES supernova fields was driven by four primary considerations:

- visibility from Cerro Tololo,
- visibility from Northern Hemisphere 8-meter class telescopes for follow-up spectroscopy,
- past observation history as it pertains to the

use of pre-existing galaxy catalogs and calibration,

- overlap with the survey area for the Visible & Infrared Survey Telescope for Astronomy (VISTA, Emerson et al. 2004).

In this paper, we focus on five fields because we have selected a hybrid supernova survey strategy as the default (see the discussion below) with two deep fields and three shallow fields¹². We undertook a detailed study of a variety of candidate fields which led to the selection of the five currently favored fields shown in Tab. 3; Fig. 1 shows their location within the DES footprint.

Field (3 deg ² area)	Pointing RA&Dec (deg., J2000)
<i>Chandra</i> Deep Field S.	52.5°, -27.5°
Sloan Stripe 82	55.0°, 0.0°
SNLS D1/Virmos VLT	36.75°, -4.5°
XMM-LSS	34.5°, -5.5°
ELAIS S1	0.5°, -43.0°

Table 3:: Currently favored Dark Energy Survey supernova fields.

We define “epoch” to be a filter observation on a given date with no requirement on a source detection. In order to make realistic simulated sets of DES SN light curve observations, we defined selection cuts that each simulated light curve must individually satisfy (see Tab. 5). The cuts ensure that a DES SN light curve used for analysis is 1) well-sampled with measurements both when the light curve is rising and falling and, 2) of sufficient quality to allow for a robust distance determination which is essential for constraining cosmology.

Tab. 4 contains example signal-to-noise ratios (snr’s) for simulated DES SN light curves for the *griz* filter set subject to the cuts described above. Note how the *g*-band measurements have significantly reduced signal-to-noise beyond a redshift of ~ 0.5 and drop out all together beyond ~ 0.8 . Our investigation of a *grizY* survey option showed that 1) the *Y*-band snr barely reaches above 5 even

¹²All the DES fields are 3 deg² in area; by “shallow” and “deep” fields we mean those with shorter or longer exposure time.

Redshift range	<i>g</i> -band snr	<i>r</i> -band snr	<i>i</i> -band snr	<i>z</i> -band snr
0.0-0.1	400	794	556	555
0.1-0.2	145	260	169	114
0.2-0.3	80	147	97	57
0.3-0.4	30	70	49	31
0.4-0.5	15	47	30	23
0.5-0.6	8	33	21	18
0.6-0.7	5	23	16	14
0.7-0.8	4	17	15	12
0.8-0.9	0	13	14	10
0.9-1.0	0	11	13	10
1.0-1.1	0	9	12	10
1.1-1.2	0	7	9	11

Table 4:: Example maximum simulated signal-to-noise ratios (snr’s) in a given redshift range and for a given filter assuming a hybrid *griz* DES-SN survey representing the current default strategy.

Selection cuts for DES supernovae
1. At least 5 total epochs above a very small, but non-zero, signal-to-noise threshold
2. At least one epoch before and at least one 10 days after the <i>B</i> -band peak
3. At least one filter measurement with a signal-to-noise above 10
4. At least two additional filter measurements with a signal-to-noise above 5

Table 5:: Selection cuts that each simulated light curve must individually satisfy in order to ensure realistic simulations of DES SN capabilities.

when half of the deep *z*-band exposure time is devoted to it and 2) the *Y*-band drops below an snr of 5 at a redshift of ~ 0.7 . Thus, we elected not to use the *Y* filter for DES-SN observations.

3.2. Example light curves and SN statistics

Fig. 5 shows example DES light curves at *z* of 0.25, 0.50, 0.74, and 1.07. Particularly noteworthy is that the flux errors projected for DES SN observations are very small at lower redshifts while remaining reasonable even beyond a redshift of 1.0. The fact that the *g*-band is absent for the *z*=0.74 and 1.07 light curves highlights why high redshift supernovae only have three colors for *griz* surveys.

In addition, the lack of the “second bump” that is characteristic of Type Ia supernovae motivates why contamination of non-Ia supernovae is more problematic at higher redshifts.

Fig. 6 shows the redshift distribution for the deep, shallow, and hybrid survey strategies. We also considered an ultra-deep strategy (3 deg^2) and found that it delivers only a marginal improvement in the number of high redshift SNe while drastically reducing the total number of SNe. Thus, we did not consider it further. Fig. 6 also shows that the deep and shallow surveys exhibit a significant decrease in the number of supernovae at low- and high-redshifts, respectively, relative to the hybrid survey. The hybrid survey also retains a significant fraction of the low- and high- z SNe found in the shallow and deep surveys while avoiding a significant fraction of the selection bias of the former (see §4.1).

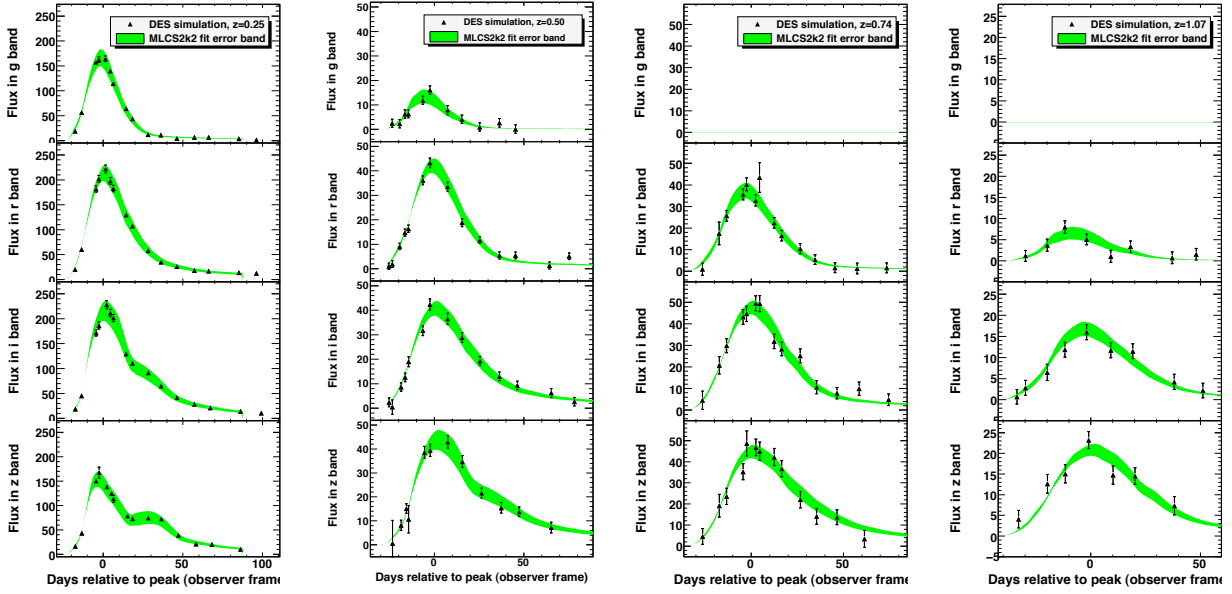


Fig. 5.—: From *left to right*: simulated DES light curve forecasts for redshifts of 0.25, 0.50, 0.74, and 1.07, respectively. Note the accuracy of the flux measurements and the reduction in strength of the g -band until it drops out altogether due to redshifting into the longer wavelength bands. The “second bump” characteristic of Type Ia supernovae is evident at lower redshifts but disappears at higher redshifts due to the fact that it is redshifted out of the z -band.

In order to explore the sensitivity of the redshift distribution to the rate of SNe Ia, we performed simulations including the α_{Ia} and β_{Ia} variations according to the uncertainties given by Eqn. 1. Since Dilday et al. (2008) found the correlation coefficient between α_{Ia} and β_{Ia} to be -0.80, we ran simulations assuming the parameters are 100% anti-correlated. We find that the projected number of DES SNe would change by approximately 7% given such a rate variation.

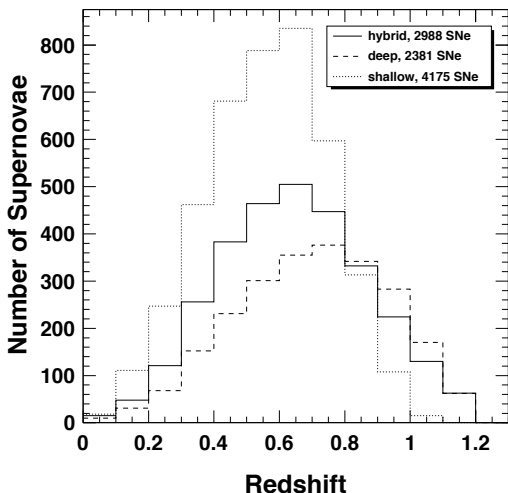


Fig. 6.—: Number of SNe vs. redshift for the DES hybrid, deep, and shallow survey strategies.

4. Supernova analysis with spectroscopic redshifts

In this section, we discuss SN Ia analysis including spectroscopic host galaxy redshifts with an emphasis on the extraction of distance estimates. In order to enhance the robustness of our results, we employ both the MLCS2k2 and SALT2 models which take fundamentally different approaches to light curve fitting (for detailed discussions, see Jha et al. 2007; Guy et al. 2007; Kessler et al. 2009b). For MLCS2k2, we consider the sub-cases of fitting both with and without priors.

4.1. MLCS2k2 light curve fitting with priors

The use of a prior on the MLCS extinction parameter A_V improves the determination of the dis-

tance modulus when the measurement error on A_V becomes wider than the width of the distribution. The improvement is noticeable in the simulated DES data at high redshift where the SN colors are determined by relatively imprecise measurements in only two bands: i and z . However, the use of a prior is prone to biases. While measurement errors, in principle, average to zero when the measurements of many SNe are combined, a bias in the prior will not average to zero. Inaccuracies in the prior, which is essentially the distribution of SNe in A_V , can arise from purely experimental errors, but unknown astrophysics including the evolution of the host galaxy population or the SN colors with redshift pose serious challenges to the use of a prior in a high precision survey like DES. While we do provide some estimate of potential systematic errors resulting from the use of a prior based on the SDSS analysis, our estimates must currently be considered tentative and incomplete.

For the analysis presented here, the prior has the following definition:

$$P_{\text{prior}} = P(A_V) \times P(\Delta) \times \epsilon_{\text{cuts}}(z, A_V, \Delta), \quad (2)$$

where $P(A_V)$ & $P(\Delta)$ are the underlying physical A_V & Δ distributions and ϵ_{cuts} is the fraction of SNe that pass the selection cuts for a given z , A_V , & Δ . For this work, following Kessler et al. (2009b), $P(A_V)$ is given by $dN/dAV = \exp(-A_V/\tau_V)$ with $\tau_V = 0.334$, and $P(\Delta)$ is an asymmetric Gaussian with peak position, Δ_0 , and positive and negative side widths, σ_+ and σ_- , respectively, given by $\Delta_0 = -0.24$, $\sigma_+ = +0.48$, $\sigma_- = +0.23$. For a given survey, e.g., the DES hybrid scenario, ϵ_{cuts} is calculated using SNANA by simulating a significant number of SN light curves (e.g., 2000) and then checking which light curves pass the defined selection cuts. Fig. 7 shows the selection efficiencies for various classes of SNe Ia. Both deep and shallow surveys are complete for nearby and/or bright SNe. However, Fig. 7 shows the benefit the hybrid survey can gain by averaging the deep and shallow selection efficiencies for distant and faint and/or heavily extinguished SNe. Fig. 8a shows our application of efficiencies to correct the hybrid survey simulation in order to better recover the true distance modulus during MLCS2k2 light curve fitting with priors¹³.

¹³The SNANA suite is also capable of taking the SN search ef-

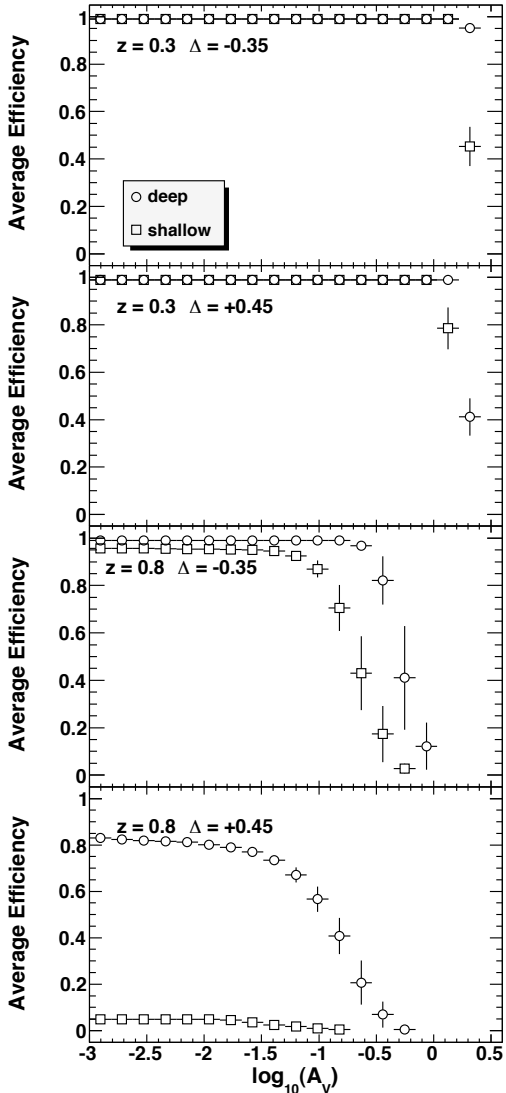


Fig. 7.—: Plotted from top to bottom is the run of efficiency with extinction parameter A_V due to the selection cuts discussed in §3.1 for DES deep and shallow fields. The efficiencies were calculated to an accuracy of 1% for a given redshift and value of Δ , A_V , and R_V . The vertical error bars show the range in efficiency for three values of R_V in a given A_V bin. For the purposes of this plot, the pre- and post-epoch cuts were disabled. This was done in order to show the efficiencies without edge effects which reduce the peak efficiencies by approximately 10-15% for the cases in the top three panels.

As discussed above, the introduction of priors can easily lead to biases if the effects of the survey signal-to-noise selection efficiency are poorly understood. Of particular concern is the bias manifested as a difference between observed (i.e. “fitted”) and true (i.e., “simulated”) distance modulus (“ μ_{fit} ” and “ μ_{sim} ” hereafter) that can arise. Fig. 8d shows such a departure of $\mu_{\text{fit}} - \mu_{\text{sim}}$ from zero beyond $z \sim 0.7$. The bias arises from not accounting for the selection efficiency in the prior and illustrates the worst case scenario for the magnitude of the μ -correction that will be needed for observational DES SN data. Note, one does not expect the selection bias to have a significant effect at low redshift because there the SN sample is essentially complete. The fact that A_V is driven toward zero, while the trend in Δ is negative, as redshift increases beyond ~ 0.5 (see Fig. 9), implies that only less extinguished and/or brighter supernovae pass the selection cuts, and strongly supports our identification of the bias in μ as a selection bias. Fig. 8d also shows, when compared to Fig. 8f, that the hybrid survey avoids a significant portion of the bias suffered by the shallow survey; recall that the hybrid survey offers a substantial improvement in statistics relative to the deep survey as well (see Fig. 6). Fig. 8e, showing the case of the deep strategy, is included for completeness. This is relevant to our selection of the hybrid strategy as our default option for the DES SN survey.

4.2. Light curve fitting without priors: MLCS2k2 & SALT2

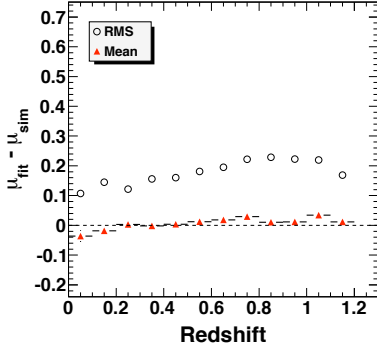
In this section, we discuss two methods of fitting without priors: flat-prior MLCS2k2 and SALT2. Such fits avoid the issue of selection efficiency bias discussed above. The trade-off is an increase in the RMS spread in the distance modulus, as is clearly evident in the comparison of Fig. 8a with Fig. 8b. In addition, Fig. 8b shows a high redshift μ bias evident in MLCS2k2 fits without priors.

The SALT2 light curve fitter in SNANA is accompanied by a separate program called SALT2mu that determines cosmological parameters and the mean relationship between the light curve parameters (m_B , x_1 , and x_3) and the distance modulus. The

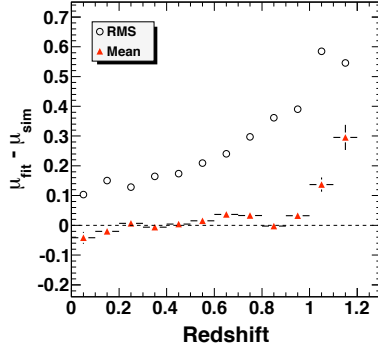
efficiency into account as was done for the SDSS SN analysis (see §6.2 in Kessler et al. 2009b); we will eventually do this for DES.

parameters that correlate distance modulus with x_1 (a stretch-like parameter) and x_3 (the excess color) are denoted as α and β respectively. We have chosen to fit for the α and β parameters independently of the cosmology using a technique that is outlined in Appendix A. Using this technique allows us to apply the same cosmological fitting procedure to the outputs of the `MLCS2k2` and `SALT2` light curve fitters.

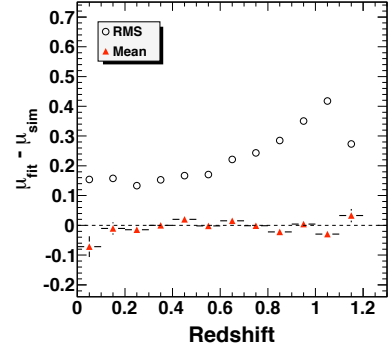
The resulting distance moduli are shown in Fig. 8c. The trend in the RMS spread of the distance modulus is rather similar to that obtained with `MLCS2k2` with the use of a flat prior. While it would be possible to apply a prior on the color in the `SALT2` fit, we have followed normal practice in not doing so here. For the majority of the remainder of this paper, we will use `MLCS2k2` fits with priors in our analyses. However, in §??, we will include `SALT2` in the discussion of DES-SN cosmology fits.



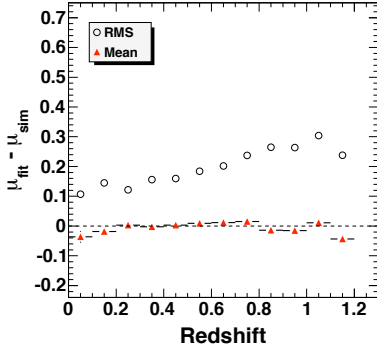
(a) MLCS2k2 fit for hybrid strategy with default priors.



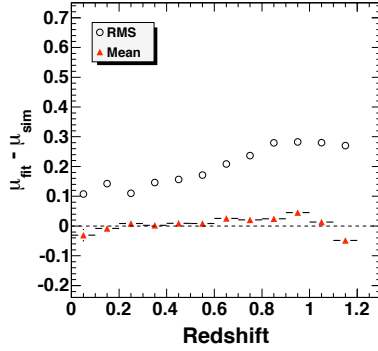
(b) MLCS2k2 fit for hybrid strategy with flat priors.



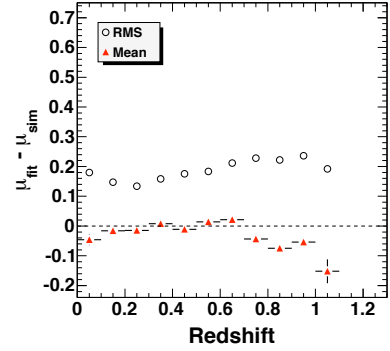
(c) SALT2 fit for hybrid strategy.



(d) MLCS2k2 fit for hybrid strategy with prior without efficiencies applied.



(e) MLCS2k2 fit for deep strategy with prior without efficiencies applied.



(f) MLCS2k2 fit for shallow strategy with prior without efficiencies applied.

Fig. 8.—: Plotted is the redshift run in $\mu_{\text{fit}} - \mu_{\text{sim}}$ for different SN light curve fitting scenarios. Dashed lines are drawn at zero for clarity.

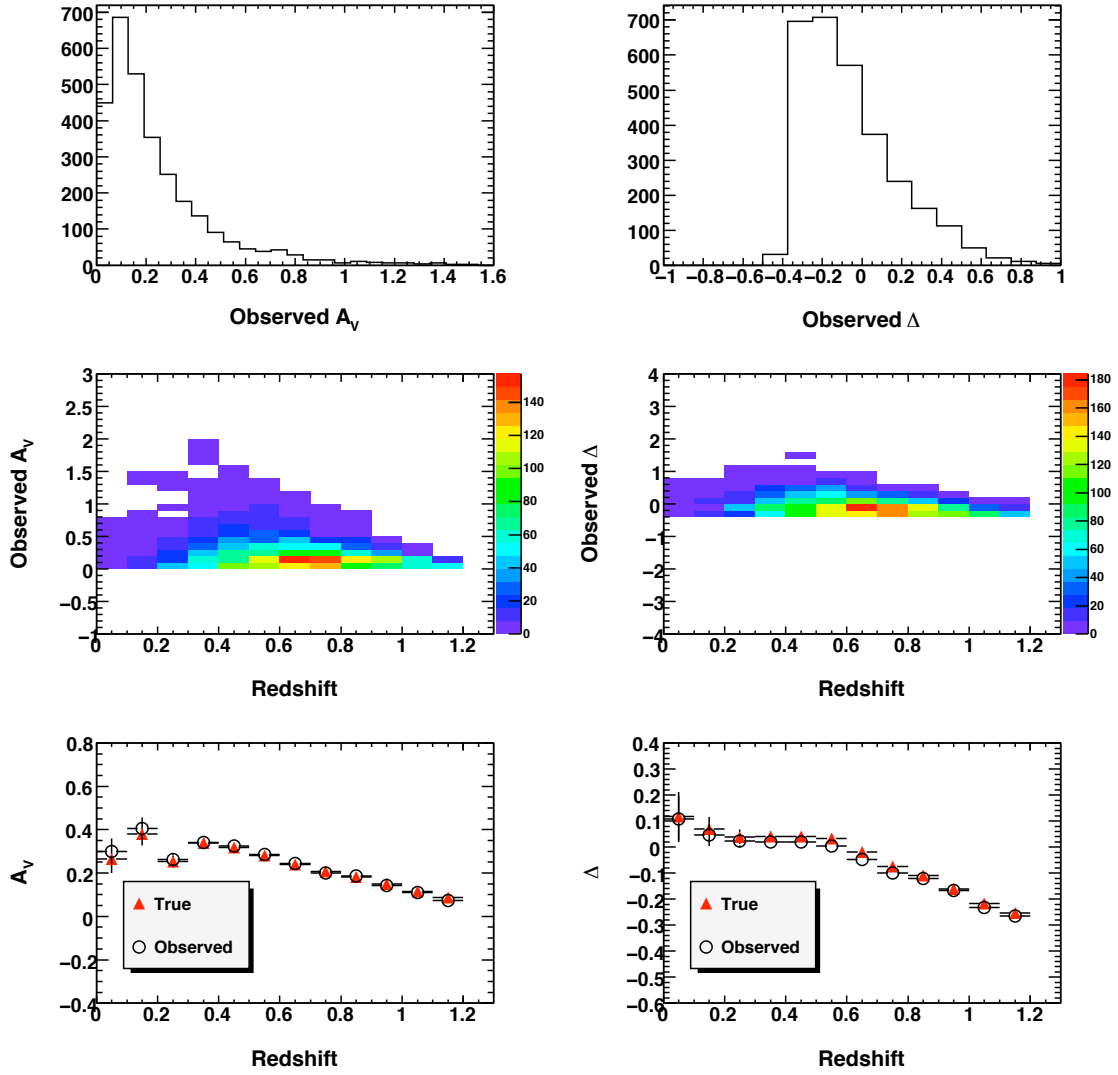


Fig. 9.— *Left:* plotted from top to bottom is the fitted (“observed”) A_V histogram and the redshift run of the observed A_V 2-D map and simulated (“true”) & observed A_V . *Right:* plotted from top to bottom is the observed Δ histogram and the redshift run of the observed Δ 2-D map and true & observed Δ . Note that the lowest redshift bin has low SN statistics (see Fig. 6).

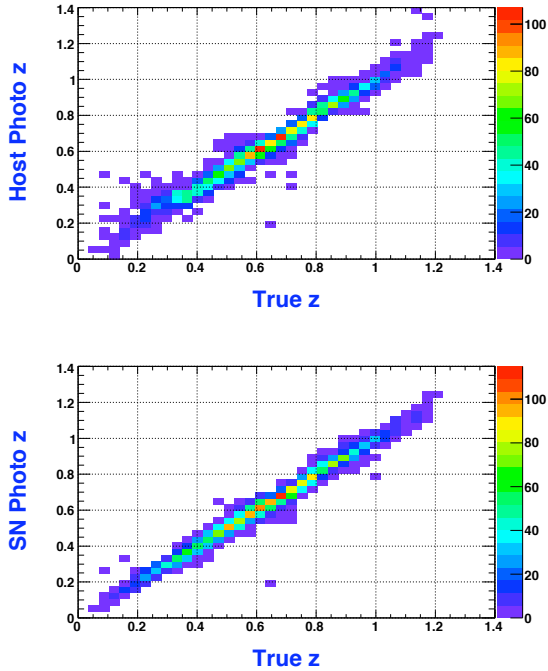


Fig. 10.— *Top*: the estimated host galaxy photo- z is plotted versus the true redshift, with colors representing the number of supernovae per bin. *Bottom*: the supernova photo- z (with the host galaxy photo- z used as a prior in the fit) is plotted versus the true redshift.

5. Photometric redshifts

A key aspect of supernovae surveys is the redshift measurement. There are four possibilities: 1) spectroscopic follow-up of an individual supernova, 2) spectroscopic measurement of the associated host galaxy, 3) photometric measurement of the supernova, and 4) photometric measurement of the host galaxy. Traditionally cosmology constraints have been performed with the full spectrum of each supernova to ensure Type Ia identification, but this will be impractical for future large surveys such as DES and LSST. The DES expects to obtain spectra for $\sim 20\%$ of the supernova sample, and this subset will be analyzed independently of the full sample to check for consistency. The spectroscopic sample will also be used to study the accuracy of photometric redshifts (photo- z 's) and sample contamination. The

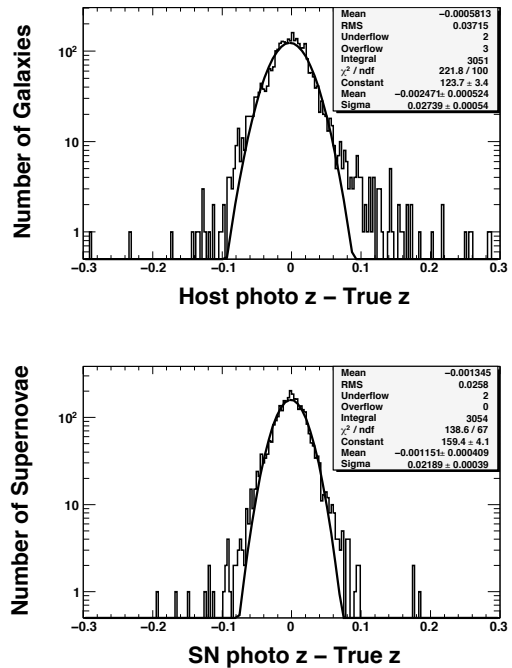


Fig. 11.— *Top*: histogram of host galaxy photo- z minus the true redshift. *Bottom*: histogram of supernova photo- z (with the host galaxy photo- z used as a prior in the fit) minus the true redshift.

full sample, however, will depend heavily on host galaxy redshifts. One of the important criteria in the choice of supernova fields discussed above was past observation history and pre-existing galaxy catalogs. These catalogs will be supplemented by other follow-up measurements to provide as close as possible to 100% of the host galaxy spectroscopic redshifts. This is the assumption for the default survey strategy, but will obviously require significant time to realize and, therefore, the use of photometric redshifts has been studied for use in the interim.

The photometric redshifts used by DES are a combination of host galaxy photo- z and supernova photo- z measurements. The host galaxy photo- z is expected to be relatively accurate since each supernova field will be sampled more than one hundred times, with an approximately two hour exposure across all filters each time, over the five-year survey. The host galaxy photo- z is determined by a neural-net algorithm described in Oyaizu et al.

(2008), and the error is estimated by the Nearest Neighbor Error estimator from the same reference. Figs. 10 & 11 show a scatter plot of photometric vs. true redshifts and the histograms for the difference of host/supernova photometric redshifts and true redshifts, respectively. The host galaxy photo- z 's have a Gaussian sigma of $\sim 2.7\%$ and a non-Gaussian tail. The supernova photo- z is fit with SNANA using the host galaxy photo- z as a prior, and is seen to have a Gaussian sigma of $\sim 2.2\%$ and much-reduced tails. In later sections, we will explore the impact on cosmology constraints if this combined photo- z fit is used instead of host galaxy spectroscopic redshifts.

A. Determination of the SALT2 α and β parameters

The α and β parameters are determined by the criterion that the scatter of distance moduli around the the Hubble curve should be minimal. We define an expression

$$\chi^2 = \sum_{i=1}^N \left[\frac{m_{Bi} - m_0(z_i) - \mu(z_i) + \alpha(z_i)x_{1i} - \beta(z_i)x_{3i}}{\sigma_i} \right]^2 \quad (\text{A1})$$

where the the functions m_0 , α , and β are chosen to minimize χ^2 and m_{Bi} , x_{1i} and x_{3i} are the fitted SALT2 parameters for the i^{th} SN. The denominator (σ_i) is the error on the quantity in the numerator and N is the number of SNe. In this paper we assume that $\alpha(z)$ and $\beta(z)$ are constants and that $m_0(z)$ is constant in each of several redshift bins. The procedure assumes a cosmology to calculate the distance modulus, but the fit is insensitive to any plausible cosmology as long as the DES data are placed in 10 (or more) redshift bins. After the parameters α and β are determined by the minimization of χ^2 the distance moduli are calculated according to

$$\mu_i = m_{Bi} + \alpha x_{1i} - \beta x_{3i} \quad (\text{A2})$$

REFERENCES

- Astier, P. et al. 2006, *A&A*, 447, 31
- Baron, E., Nugent, P. E., Branch, D., & Hauschildt, P. H. 2004, *ApJ*, 616, L91
- Bazin, G. et al. 2009, *A&A*, 499, 653
- Bessell, M. S. 1990, *PASP*, 102, 1181
- Cappellaro, E., Evans, R., & Turatto, M. 1999, *A&A*, 351, 459
- Cardelli, J. A., Clayton, G. C., & Mathis, J. S. 1989, *ApJ*, 345, 245
- Di Carlo et al. 2002, *ApJ*, 573, 144
- Dilday, B. et al. 2008, *ApJ*, 682, 262
- Emerson, J. P., Sutherland, W. J., McPherson, A. M., Craig, S. C., Dalton, G. B., & Ward, A. K. 2004, *The Messenger*, 117, 27
- Freedman, W. L. et al. 2009, *ApJ*, 704, 1036
- Frieman, J. A., Turner, M. S., & Huterer, D. 2008a, *ARA&A*, 46, 385
- Frieman, J. A. et al. 2008b, *AJ*, 135, 338
- Fryxell, B., Olson, K., Ricker, P., Timmes, F. X., Zingale, M., Lamb, D. Q., MacNeice, P., Rosner, R., Truran, J. W., & Tufo, H. 2000, *ApJS*, 131, 273
- Gilliland, R. L., Nugent, P. E., & Phillips, M. M. 1999, *ApJ*, 521, 30
- Groom, D. E. et al. 2006, in *Bulletin of the American Astronomical Society*, Vol. 38, *Bulletin of the American Astronomical Society*, 1038
- Guy, J. et al. 2007, *A&A*, 466, 11
- Hamuy, M. et al. 2002, *AJ*, 124, 417
- . 2006, *PASP*, 118, 2
- Holland, S. 2002, *Experimental Astronomy*, 14, 83
- Holtzman, J. A. et al. 2008, *AJ*, 136, 2306
- Jha, S., Riess, A. G., & Kirshner, R. P. 2007, *ApJ*, 659, 122
- Kessler, R., Bernstein, J. P., Cinabro, D., Dilday, B., Frieman, J. A., Jha, S., Kuhlmann, S., Miknaitis, G., Sako, M., Taylor, M., & Vanderplas, J. 2009a, *PASP*, 121, 1028
- Kessler, R. et al. 2009b, *ApJS*, 185, 32
- Leaman, J. F., Li, W., Filippenko, A., & LOSS. 2009, in *American Astronomical Society Meeting Abstracts*, Vol. 214, *American Astronomical Society Meeting Abstracts*, #316.02—+
- Li, W., Wang, X., Van Dyk, S. D., Cuillandre, J., Foley, R. J., & Filippenko, A. V. 2007, *ApJ*, 661, 1013
- Miknaitis, G. et al. 2007, *ApJ*, 666, 674
- Nugent, P., Kim, A., & Perlmutter, S. 2002, *PASP*, 114, 803
- Oyaizu, H., Lima, M., Cunha, C. E., Lin, H., & Frieman, J. 2008, *ApJ*, 689, 709
- Perlmutter, S. et al. 1999, *ApJ*, 517, 565
- Phillips, M. M., Lira, P., Suntzeff, N. B., Schommer, R. A., Hamuy, M., & Maza, J. 1999, *AJ*, 118, 1766
- Prieto, J. L., Stanek, K. Z., & Beacom, J. F. 2008, *ApJ*, 673, 999
- Regnault, N. et al. 2009, *A&A*, 506, 999
- Richardson, D., Branch, D., Casebeer, D., Millard, J., Thomas, R. C., & Baron, E. 2002, *AJ*, 123, 745
- Riess, A. G. et al. 1998, *AJ*, 116, 1009
- Schlegel, D. J., Finkbeiner, D. P., & Davis, M. 1998, *ApJ*, 500, 525
- Smartt, S. J., Eldridge, J. J., Crockett, R. M., & Maund, J. R. 2009, *MNRAS*, 395, 1409
- Strolger, L.-G. et al. 2004, *ApJ*, 613, 200
- Thuan, T. X. & Gunn, J. E. 1976, *PASP*, 88, 543
- van den Bergh, S., Li, W., & Filippenko, A. V. 2005, *PASP*, 117, 773
- Wood-Vasey, W. M. et al. 2007, *ApJ*, 666, 694

This 2-column preprint was prepared with the AAS L^AT_EX macros v5.0.